Original Article

JCBFM

Journal of Cerebral Blood Flow & Metabolism
2018, Vol. 38(11) 1924–1939

DOI: 10.1177/0271678X18786356
journals.sagepub.com/home/jcbfm
SAGE

Nutrient limitation affects presynaptic structures through dissociable Bassoon autophagic degradation and impaired vesicle release

Alberto Catanese[1,2], Débora Garrido[1,2], Paul Walther[3], Francesco Roselli[1,4] and Tobias M Boeckers[1]

Abstract

Acute mismatch between metabolic requirements of neurons and nutrients/growth factors availability characterizes several neurological conditions such as traumatic brain injury, stroke and hypoglycemia. Although the effects of this mismatch have been investigated at cell biological level, the effects on synaptic structure and function are less clear. Since synaptic activity is the most energy-demanding neuronal function and it is directly linked to neuronal networks functionality, we have explored whether nutrient limitation (NL) affects the ultrastructure, function and composition of pre and postsynaptic terminals. We show that upon NL, presynaptic terminals show disorganized vesicle pools and reduced levels of the active zone protein Bassoon (but not of Piccolo). Moreover, NL triggers an impaired vesicle release, which is reversed by re-administration of glucose but not by the blockade of autophagic or proteasomal protein degradation. This reveals a dissociable correlation between presynaptic architecture and vesicle release, since restoring vesicle fusion does not necessarily depend from the rescue of Bassoon levels. Thus, our data show that the presynaptic compartment is highly sensitive to NL and the rescue of presynaptic function requires re-establishment of the metabolic supply rather than preventing local protein degradation.

Keywords

Autophagy, Bassoon, nutrient limitation, synapses, synaptic vesicles

Received 6 March 2018; Revised 14 May 2018; Accepted 9 June 2018

Introduction

Neuronal biology involves energy-intensive activities such as maintenance of membrane potentials, intracellular transport and protein turnover, requiring continuous metabolic support.[1] In fact, acute deprivation of metabolites results in sudden neurological dysfunction and, if sustained long enough, permanent neurological damage. Acute mismatch between the required metabolic substrates and the ones available to neurons characterizes several severe clinical conditions: in traumatic brain injury, spreading wave of depolarization induces a state of hyperglycolysis and the rapid depletion of substrates for intermediate metabolism[2]; in stroke, the sudden decrease in blood flow deprives neurons both of oxygen and of metabolic substrates[3]; in hypoglycemia-induced encephalopathy (a condition associated with excess of insulin or sulphonylurea therapy in humans),[4] glucose deprivation leads to neuronal loss even in normoxic conditions.[5]

The neuronal responses to sudden changes in nutrients availability are subject of intense investigation: upon oxygen limitation, alternative usage of glucose in

[1]Institute of Anatomy and Cell Biology, Ulm University, Ulm, Germany
[2]International Graduate School in Molecular Medicine Ulm (IGradU), Ulm University, Ulm, Germany
[3]Electron Microscopy Institute, Ulm University, Ulm, Germany
[4]Department of Neurology, Ulm University, Ulm, Germany

The first two authors contributed equally to this work.
The last two authors are co-senior authors.

Corresponding author:
Tobias M Boeckers, Department of Anatomy and Cell biology, School of Medicine, Ulm University, Albert-Einstein-Allee 11, Ulm DE 89081, Germany.
Email: tobias.boeckers@uni-ulm.de

pentose phosphate pathway rather than in the glycolytic pathway provides increased resilience to neuronal death.[3] Likewise, sudden deprivation of nutrients and growth factors activates autophagic degradation in neurons.[6]

However, despite synaptic vesicle (SV) cycling and postsynaptic potentials are the most energy-demanding function in the CNS,[1,7] very little is known about how synapses react to sudden nutrient limitation (NL). Indeed, disruption of glucose influx into presynaptic terminals is sufficient to prevent SV endocytosis and recycling, preventing repetitive firing.[8] Nevertheless, the broad consequences of NL on the architecture of synaptic terminals, and their functional implications, have not been fully investigated. Scaffold proteins are fundamental organizing blocks of pre- and postsynaptic terminal architectures. In the presynapse, the multidomain scaffold proteins Bassoon and Piccolo[9,10] play an important role in tethering and priming SV to the release site: improper stoichiometry of Bassoon or Piccolo results in the decrease in vesicle release.[11] In addition, Bassoon constitutively limits autophagy in presynaptic terminals,[12] and Bassoon loss results in the ubiquitination of vesicle proteins and their removal from the presynapse.[13] On the other hand, the electron-dense postsynaptic structure of excitatory synapses (the postsynaptic density or PSD) is organized by interacting scaffold proteins such as the PSD95 (MAGUK)[14] family members and the Shank family members (Shank1, 2 and 3),[15] which regulate glutamate receptors turnover and endocytosis,[16] signaling proteins, actin cytoskeleton[17] and dendritic spine morphology.[18] PSD proteins are subject to ubiquitination[19] and are subject to an intense turnover rate, being degraded according to the rate of synaptic activity[20] in physiological conditions and upon pathogenic cues such as in neurodegenerative diseases.[21,22]

Here we have investigated the effect of NL on the synaptic levels of several pre- and postsynaptic scaffold proteins and on the overall synaptic architecture. We have found that NL induces ultrastructural and functional changes at the presynaptic sites associated with reduced Bassoon pool and, through independent mechanisms, with the significant decrease in SV release, which recovers upon nutrients re-supply.

Material and methods

Animal ethics statement

All animal experiments in this study were approved by the review board of the Land Baden-Württemberg (Permit Number Nr. O.103) and performed in compliance with the ARRIVE Guidelines and with the guidelines for the welfare of experimental animals issued by the Federal Government of Germany and the Max Planck Society. Sprague-Dawley rats were purchased from Janvier Labs.

Cell culture and NL protocol

Primary cultures of rat hippocampal neurons were prepared from rat embryos (Sprague-Dawley rats, Janvier Laboratories) at E17–18 as described previously and detailed in Supplementary Methods.[23,24] Experiments were performed at 14 days in vitro (DIV14). According to previously published reports in which no mitotic inhibitor was used to limit glial proliferation,[25,26] with this protocol we generated mixed cultures of neurons (70%) and astrocytes (30%), for brevity referred to as "neuronal culture."

In the nutrient-limitation (NL) experiments, NB^+ medium was replaced with Hank's Balanced Salt Solution (HBSS) for 1, 3, 5, or 10 h. HBSS is commonly used as NL medium for a large number of cell types, including neurons.[27–31] Concentration of D-Glucose in HBSS was 5.555 mM (for comparison, 25 mM in Neurobasal), and therefore compared to DMEM or Neurobasal-based starvation media simulates a reduced availability of glucose, aminoacids and growth factors. For nutrients re-establishment experiments (time course shown in Figure 2(e)), HBSS was replaced in each well after 5 h by the corresponding conditioned NB medium for 2 or 5 h. Conditioned medium was previously collected at the beginning of the experiment and kept at 37°C.

The autophagy inhibitor 3-Methyladenine (3-MA, final concentration 10 mM, InvivoGen) or the proteasome inhibitor Bortezomib (PS-341, final concentration 0.1 μM, Selleck Chemicals) was added to the culture medium (NB^+ or NL) for 5 h.[32,33] Control cultures were treated with 0.1% DMSO as vehicle control.

In the NL-recovery experiment, neurons were exposed to NL treatment for 3 h and then either glucose (addition of 19.445 mM to reach a final concentration of 25 mM as in Neurobasal medium), the alanine-glutamine dipeptide (GlutaMAX, Gibco; 1%), glutamine (Gibco; 1%), BDNF (0.02 μg/ml) or Insulin (0.6 μM)[6] was added to HBSS for 2 h. In the last 30 min of the experiments, cells underwent anti-Synaptotagmin-1 antibody uptake assay (see below), fixed and processed for immunostaining.

The same protocol was applied to evaluate the contribution of autophagy in the NL-recovery mediated by single nutrient re-supplementation by inhibiting the degradative pathway: after 3 h of NL, the alanine-glutamine dipeptide, 3-MA or the combination of the two was added to HBSS for 2 h. Cells were then processed as described above.

Anti-synaptotagmin-1 antibody feeding protocol

The SV release rate was analyzed using the anti-synaptotagmin antibody feeding protocol, as previously reported.[34] Briefly, hippocampal neurons were exposed for 30 min (from 4.5 to 5 h in the NL experiment and in the recovery experiment) to a culture medium (either NB^+ or NL) containing a monoclonal antibody (diluted 1:500) directed against a luminal epitope of Synaptotagmin-1 fluorescently labeled with Oyster®550 (105 103C3, Synaptic System). At the end of the antibody-feeding step, cells were washed twice in PBS and were fixed with 4% paraformaldehyde/4% sucrose for 10 min. After washing, the cells were processed for immunostaining procedure (see Supplementary Methods).

For the stimulated SV assay, hippocampal neurons (cultured either in NB^+ or HBSS) were incubated for the last 5 min of the experiments with the respective medium in presence/absence of KCl 55 mM and anti-Synaptotagmin-1 antibody, as previously reported.[35] Cells were then processed as reported above.

Primary antibodies

The list of commercial primary antibodies is reported in Supplementary Methods. The Rb anti-Shank2 and Rb anti-Shank3 antibodies were available in our laboratory and produced as previously described.[36,37]

Western blot

Western blot of whole-cell protein extracts was performed as previously reported[24]; the detailed protocol is reported in Supplementary Methods.

Immunostaining

Immunocytochemistry (ICC) was performed as described previously[24,38] with minor modifications. The detailed protocol is reported in Supplementary Methods.

Fluorescence microscopy and image analysis

An upright Axioscope 2 microscope equipped with a Zeiss CCD camera (16 bits; 1280 ppi × 1024 ppi) and either a 20 × air or a 63 × oil immersion objective was used to acquire single-plane fluorescence images using Axiovision software (Zeiss). Identical imaging settings were applied to each experimental group among individual experiments. To ensure the blind evaluation of the images, pictures were acquired by an author (DG) but analyzed by another author (AC) unaware of the treatment group. For the assessment of neuronal survival upon NL, the number of $MAP2^+$ cells displaying an identifiable nucleus (stained with DAPI) and clearly identifiable processes was counted in five randomly selected fields (acquired using a 20× objective) from two coverslips per condition from each of the three independent cultures. We considered apoptotic those neurons showing fragmented nuclei and condensed chromatin, as previously reported.[39,40]

To analyze the density and the size of synaptic markers, images acquired with the Axioscope microscope were analyzed with ImageJ software as previously reported.[21,22] From each culture replicate (each culture corresponding to an independent experiment, $n = 3$), for each conditions, we selected randomly 10–15 neurons from each coverslip, and 2–3 coverslips per groups were considered; altogether, data shown come from 45–90 neurons per experimental group. Selection of the neurons was performed in the MAP2 channel to avoid selection bias. From each neuron, three different randomly selected 30 µm-long artifact-free dendrites were considered. Synaptic clusters were identified according to their proximity to the $MAP2^+$ dendrite and to the minimal size of 0.1 μm^2. Images were intensity-thresholded (threshold was selected for each synaptic protein according to the signal-to-noise ratio and kept constant across replicates) and individual clusters were manually traced and their size was logged. In Shank2-overexpressing neurons, dendrites were identified according to their morphology in the GFP channel. For the analysis of Synaptotagmin-1 clusters (total number and mean intensity), we used the plug-in Find Foci for ImageJ[41] and MaxEntropy threshold algorithm.

Confocal images were acquired at the resolution of 1024 × 1024 pixels using a Leica DMi8 laser-scanning microscope equipped with an ACS APO 63 × oil immersion objective and optical section thickness of 0.2 µm.

Dendritic spines morphology in Life-Act-expressing hippocampal neurons[22,42] was analyzed using Imaris software (Bitplane) in confocal images deconvolved with AutoQuant X software (MediaCybernetics). The dendritic tree was reconstructed using the Filament Tracing tool in Imaris. Spines were then identified with the corresponding wizard (Spine detection) using default settings (Seed point 0.455 µm; Max length 4 µm), allowing detection of branched spines and keeping constant the threshold values within independent experiments. The spine morphology was performed using Classify Spines Xtension (Bitplane) using default settings.

The colocalization between Atg5 and Bassoon was quantified using the Spot detection tool in Imaris (Bitplane). Briefly, puncta for each protein were detected semi-automatically in the respective channel and the interaction between the two markers was accepted within a minimum distance between the respective spots of 0.3 µm. All the experiments were performed in minimum of three independent replicates,

and at least 10 cells per condition were analyzed (three dendrites for each neuron). Images were manipulated applying the same parameters for figure display.

Transmission electron microscopy, scanning transmission electron microscopy tomography, and quantitative analysis

Transmission electron microscopy (TEM) was performed as previously reported[43]; the detailed protocol is reported in the Supplementary Methods.

For scanning transmission electron microscopy (STEM), tomography samples were prepared as for TEM (see Supplementary Methods) but the sections were cut at a microtome setting of 600 nm. The STEM-tomograms were acquired with a Jeol 2100F at 200 kV using the brightfield STEM mode as described by Villinger et al.[43] For STEM-tomography, the specimens were tilted from -72° to 72° with 1.5° increment. Reconstruction of the tomogram from the tilt series and the 3D model was performed with the IMOD software.[44]

Images were acquired in a Jeol JEM 1400 transmission electron microscope at a magnification of $80{,}000\times$. Only artifact-free synapses, with clearly identifiable PSD, presynaptic and postsynaptic terminals were selected for analysis. The PSD area, length and thickness were measured using ImageJ software applying a constant threshold as previously reported.[21,45] For the analysis of the SV density, vesicles number and presynaptic terminal size were manually traced in ImageJ. Synaptic clustering was assessed by the number of intersections between SV profiles and a superimposed grid (5 μm mesh). The normalized number of vesicles was divided by number of intersections to compute the "distribution index." Autophagosomes were identified as round-shaped vesicles surrounded by a double-membrane and showing either electron-dense or empty lumen according to published criteria.[46,47]

Statistical analyses

Data collection and statistical analysis were performed using Microsoft Excel and GraphPad Prism (Version 7). All the data presented derive from three independent experiments (neuron preparations) including always the respective controls.

Statistical analysis was performed as follow: unpaired *t* test with Welch's correction and non-parametric Mann–Whitney test were used to compare two independent groups (Control vs. NL); one-way ANOVA followed by Sidak's post hoc test was used to evaluate differences among multiple independent groups. Statistical significance was set at $p < 0.05$. Data are presented as *fold change* relative to the respective control/baseline (if not differently stated in the figure legends), and error bars indicate standard deviation (SD).

Results

In vitro NL suppresses mTOR phosphorylation and activates autophagy

In order to investigate how the structure and function of synaptic contacts are affected by the sudden limitation of metabolic substrates, we exploited an in-vitro NL model (previously reported by Young et al.[6] and Maday et al.[48]). Rat hippocampal neurons (DIV 14) were exposed to HBSS in normoxic culture conditions for 5 h. We confirmed the response of the neurons to NL demonstrating that, despite no change in the total amount of mTOR and Akt (Figure 1(a)), 5 h NL caused a significant decrease of phosphorylated mTOR (Ser2448; NL: 0.468 ± 0.235 fold of Control, $p = 0.0458$) as well as of phosphorylated Akt (Thr308; NL: 0.348 ± 0.101 fold of Control, $p = 0.0098$) in comparison to neurons kept in NB^+ medium (Figure 1(b)).[49] Likewise, NL upregulated the autophagic flux, as revealed by the significant increase in the number of the autophagic receptor p62 clusters located within the cell somata (NL: 1.536 ± 0.175 fold of Control, $p = 0.0497$; Figure 1(c)), while the total levels of p62 (WB of whole-cell protein extract) were reduced in NL neurons (NL: 0.419 ± 0.080 fold of Control, $p = 0.0474$; Figure 1(d)). Since p62 is recruited to the autophagosomes and subsequently degraded via lysosomes, these data confirmed that NL enhanced the autophagic flux.[50] Nevertheless, 5 h of NL did not cause any significant decrease in the numbers of neurons in culture (Figure 1(e)). These findings suggest that neurons can set in motion a coordinated and effective response to NL without loss of cell viability.

NL activates autophagy specifically at synaptic sites

Next, we explored how NL affected the stability of key synaptic assemblies in the pre- and postsynaptic compartment. Hippocampal neurons fixed after 5 h-NL (or from control conditions) were immunostained for MAP2 for dendrite identification and for presynaptic (Bassoon, Piccolo) and postsynaptic (Shank2, Shank3, Homer, NR1 and Gephyrin) proteins. Interestingly, both the number and the size of Bassoon clusters were significantly reduced by NL (NL clusters number: 0.485 ± 0.126 fold of Control, $p = 0.0316$; clusters size: $0.266 \pm 0.235\,\mu m^2$ in Control vs. $0.218 \pm 0.179\,\mu m^2$ in NL, $p < 0.0001$; Figure 2(a)), whereas the number and the size of Piccolo clusters were unaffected (Figure 2(b)). Surprisingly, NL did not affect the size or

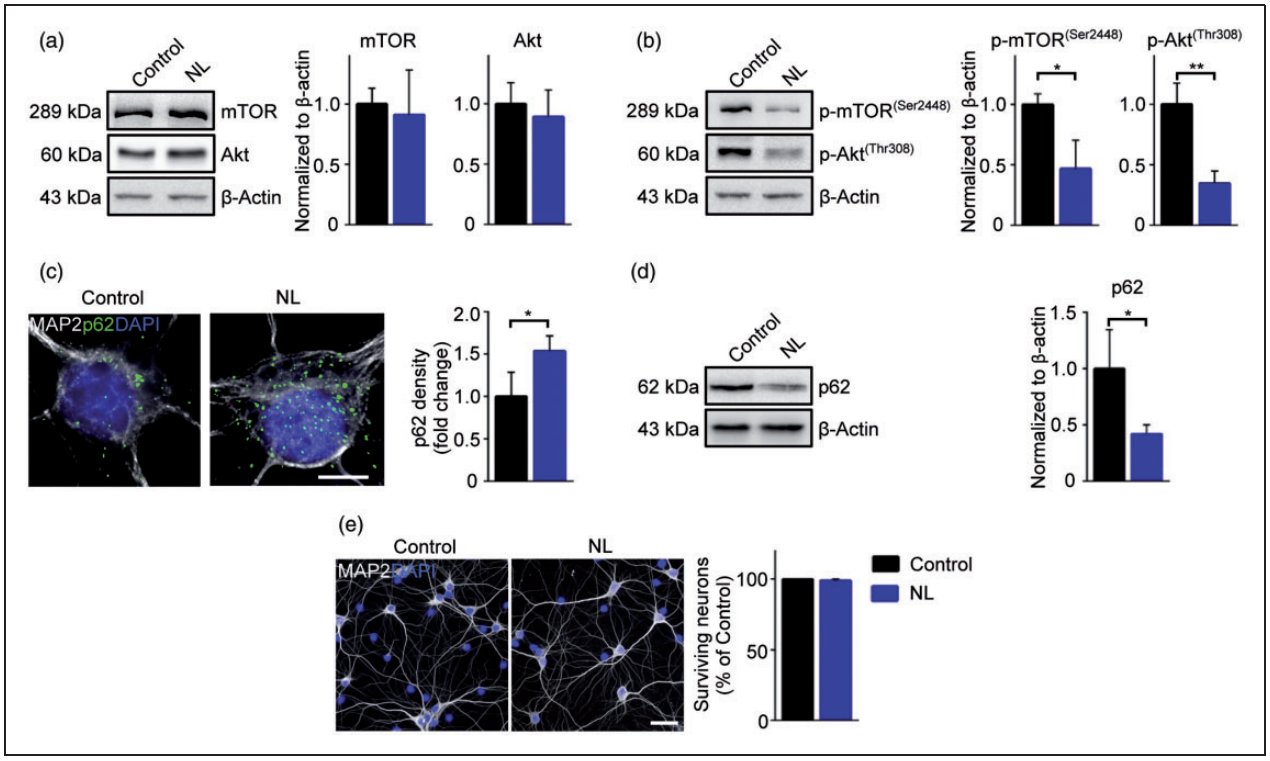

Figure 1. NL activates mTOR-dependent autophagy without causing neuronal death. (a and b) Representative immunoblots and quantitative analysis of total (a) and phosphorylated (b) mTOR (Ser2448) and Akt (Thr308). The phosphorylation levels are reduced in NL neurons (Control vs. NL: p-mTOR $p = 0.0458$; p-Akt $p = 0.0098$) (c) Representative images of neuronal somata showing increased accumulation of p62 puncta number upon NL (Control vs. NL $p = 0.0497$) (d) Representative immunoblots and quantitative analysis showing reduced levels of total p62 in NL neurons (Control vs. NL $p = 0.0474$) (e) Representative wide field images showing that 5 h NL does not induced neuronal loss, as detected by absence of apoptotic neurons. Experiments were performed in $N = 3$ independent replicates. Data are displayed as Mean ± SD. (*$p < 0.05$, **$p < 0.01$). Scale bars represent 10 μm in (c) and 50 μm in (e).

cluster density of the scaffold proteins Shank2, Shank3, Homer1, as well as the total levels of Shank2 isoforms and PSD95 from whole-cell lysates (Supplementary Figure S1(a) to (e)). Interestingly, while NL did not alter the number of glutamate receptor NR1 clusters, it induced an increase in their size (clusters size: $0.293 \pm 0.341\ \mu m^2$ in Control vs. $0.344 \pm 0.414\ \mu m^2$ in NL, $p < 0.0001$; Figure 2(c)). In addition, NL did not alter the number but caused a significant decrease of Gephyrin$^+$ cluster size in NL neurons (clusters size: $0.296 \pm 0.248\ \mu m^2$ in Control vs. $0.249 \pm 0.244\ \mu m^2$ in NL, $p < 0.0001$; Figure 2(d)).

Notably, we observed a minor, but not significant reduction of Shank2 cluster density after 10 h of NL (Supplementary Figure S1(f)). Moreover, the postsynaptic scaffold protein Homer showed no significant change in its cluster density after 10 h of NL (Supplementary Figure S1(g)). This suggested that PSD composition is affected later than the presynaptic active zone under prolonged stress conditions.

Because of the critical role of Bassoon in regulating the architecture of presynaptic terminals,[51] we mapped the time course of its disappearance under NL: decrease in Bassoon cluster density was already detected after 1 h of NL (1 h NL: 0.894 ± 0.069 fold of baseline), and it significantly further decreased after 3 (3 h NL: 0.762 ± 0.049 fold of 1 h NL, $p = 0.004$) and 5 h of NL (5 h NL: 0.722 ± 0.126 fold of 3 h NL, $p = 0.0117$; Figure 2(e)), suggesting a progressive loss. We compared Bassoon loss with the kinetics of NL-induced p62 accumulation: although only a minor increase in the density of p62$^+$puncta after 1 and 3 h of NL, a dramatic increase in p62 clusters was detected at 5 h (5 h NL: 1.754 ± 0.202 fold of baseline, $p = 0.0127$; Figure 2(e)). On the other hand, re-incubation of NL neurons with their respective NB$^+$ conditioned medium (see Material and Methods) rapidly reverted autophagic induction (density of p62 clusters 2 h after re-incubation was comparable to the one at baseline, $p = 0.6$), whereas Bassoon levels returned close to baseline level only after 5 h, even though they appeared still reduced compared to control (5 h NL + 5 h nutrient re-establishment: 0.862 ± 0.092 fold of baseline, $p = 0.0489$). Taken together, these data show that the kinetics of Bassoon degradation is faster than the average autophagic flux in the cell body, whereas restoration of Bassoon takes

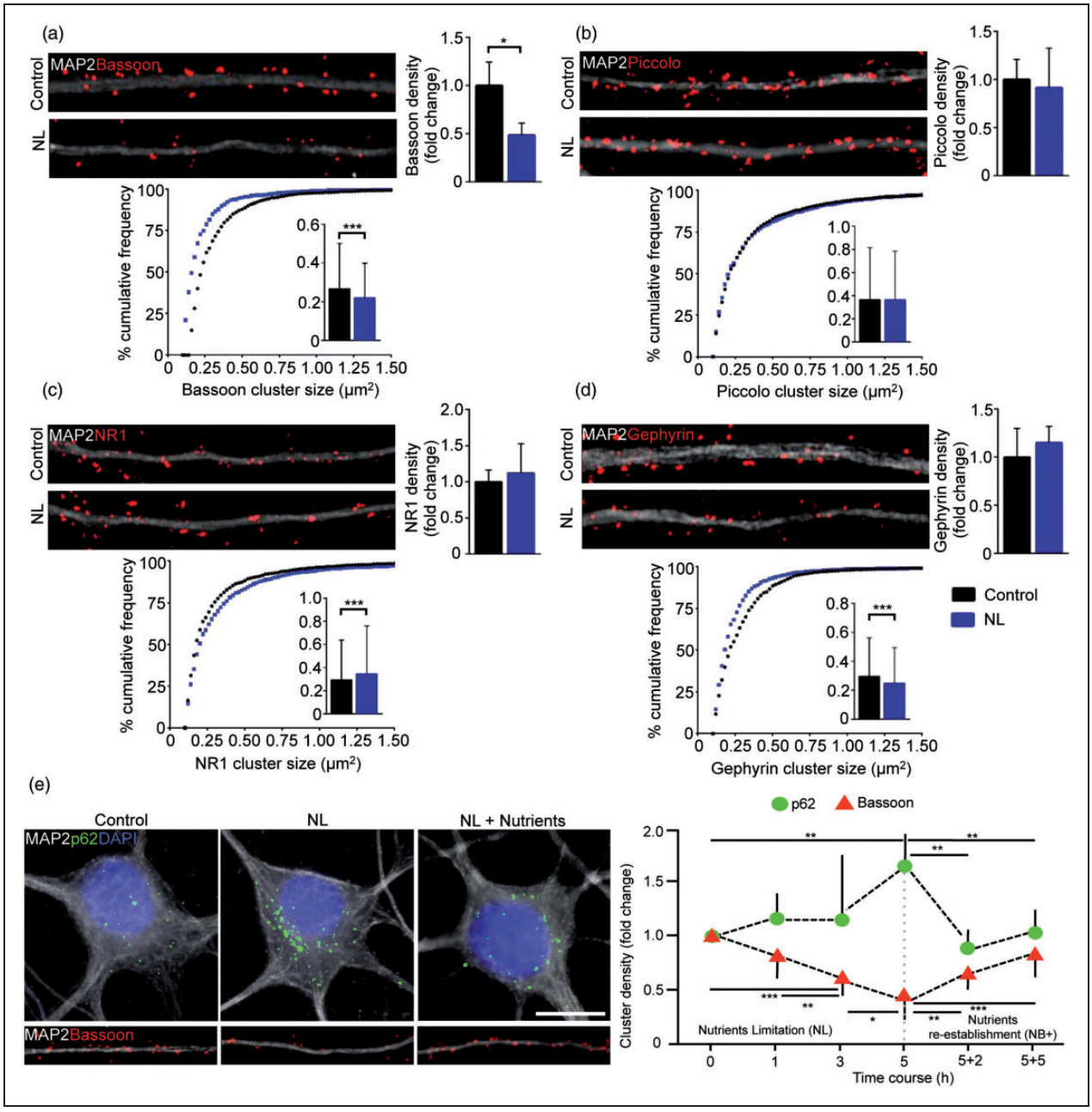

Figure 2. Synaptic autophagy induces drastic loss of Bassoon. (a, b, c and d) Representative images of dendrites (30 μm) from Control and NL neurons immunostained against MAP2 and Bassoon (a), Piccolo (b), NR1 (c) Gephyrin (d). NL reduces Bassoon clusters number (Control vs. NL $p = 0.0316$) and size (Control vs. NL $p < 0.0001$), but does not affect Piccolo. NL neurons show increased size of NR1 clusters (Control vs. NL $p < 0.0001$); and smaller Gephyrin clusters (Control vs. NL $p < 0.0001$). (e) Time course analysis of p62 and Bassoon kinetics upon NL (p62: 0 h vs. 5 h NL $p = 0.0036$; 5 h NL vs. 5 h NL + 2 h NB$^+$ $p = 0.0012$; 5 h NL vs. 5 h NL + 5 h NB$^+$ $p = 0.0036$. Bassoon: 0 h vs. 3 h NL $p = 0.0002$; 0 h vs. 5 h NL $p < 0.0001$; 0 h vs. 5 h NL + 2 h NB$^+$ $p = 0.0012$; 0 h vs. 5 h NL + 5 h NB$^+$ $p = 0.0489$; 1 h vs. 3 h NL $p = 0.004$; 1 h vs. 5 h NL $p < 0.0001$; 3 h vs. 5 h NL $p = 0.0117$; 3 h vs. 5 h NL + 5 h NB$^+$ $p = 0.0101$; 5 h NL vs. 5 h NL + 2 h NB$^+$ $p = 0.0017$; 5 h NL vs. 5 h NL + 5 h NB$^+$ $p < 0.0001$). Experiments were performed in N = 3 independent replicates. Data are displayed as Mean ± SD. (*$p < 0.05$, **$p < 0.01$, ***$p < 0.001$). Scale bar represents 10 μm in (e).

place significantly slower than the nutrient suppression of autophagy.

Since the effect of NL appeared more pronounced on the presynaptic terminal composition, we investigated functional change in vesicle release upon NL. Control and NL cultures were subject to anti-synaptotagmin 1 (Syt1) uptake assay under baseline culture condition and after 55 mM KCl depolarization.[34,35] At baseline,

the intensity and the number of presynaptic terminals labeled by anti-Syt1 antibody were already reduced in NL neurons (NL baseline clusters intensity: 0.820 ± 0.017 fold of Control baseline, $p = 0.0001$; NL baseline clusters number: 0.450 ± 0.132 fold of Control baseline, $p = 0.0464$). Moreover, the intensity of labeled terminals was strongly increased by KCl depolarization in Control conditions (Control+KCl 55 mM clusters intensity: 1.113 ± 0.012 fold of Control baseline, $p = 0.004$; Control+KCl 55 mM clusters number: 1.6 ± 0.265 fold of Control baseline, $p = 0.0225$; Figure 3), whereas NL neurons failed to increase vesicle release upon depolarization. Thus, NL displays a significant effect on specific proteins of presynaptic terminals, leading to the impairment in SV release, without apparently affecting major excitatory postsynaptic proteins.

TEM reveals reduced SV clustering upon NL

We further investigated the changes imposed by NL on the architecture of the presynaptic terminal at ultrastructural levels exploiting high-pressure freezing fixation[43] to best preserve synaptic ultrastructure, followed by TEM of thin sections from hippocampal cultures subject to NL (or to NB^+). Only synaptic terminals in which both the pre- and postsynaptic terminals were identifiable in the same TEM image were considered for analysis. At presynaptic level, no obvious signs of degeneration (plasmalemmal breakdown, inflated mitochondria, diffuse vacuolization) were detected in NL compared to NB^+ or samples. However, the clustering of SVs was significantly decreased (expressed as distribution index, see Material and Methods) in NL samples compared to Control conditions (NL: 0.694 ± 0.432 fold of Control, $p = 0.0465$; Figure 4(a) and (b)), whereas the total number of SV per bouton was comparable between the two treatments. In addition to the reduced density of SV, NL neurons showed a strong reduction of docked SV at the presynaptic bouton (number of SV per 500 nm active zone: Control 3.35 ± 2.246 vs. NL 1.946 ± 2.197; $p < 0.0001$). Notably, NL did not significantly alter neither the structures at the postsynaptic site, nor any morphological parameter of the PSD (data not shown). Interestingly, the NL postsynaptic sites displayed a significantly increased frequency of autophagic vesicles (AVs, identified as double-membrane vacuoles according to recently published criteria)[46,47] compared to Control (AVs frequency: 0.124 ± 0.364 in Control vs. 0.382 ± 0.791 in NL, $p = 0.0148$; Figure 4(b) and (c)). In contrast, the presynapses did not show any increase in the AVs frequency at this time point (5 h of NL) compared to Control.

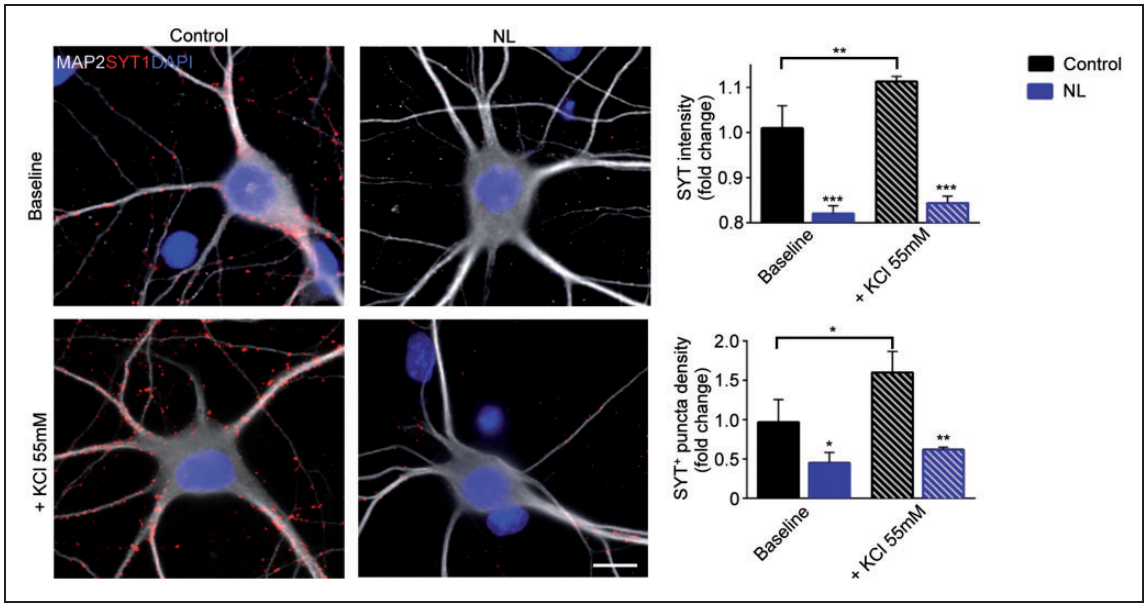

Figure 3. NL reduces the release of synaptic vesicles. Anti-Synaptotagmin-1 antibody uptake assay was performed in Control and NL neurons in basal condition or under KCl-mediated depolarization. Control neurons stimulated with 55 mM KCl for 5 min show a drastic increase of Syt1 puncta intensity (Control baseline vs. Control KCL 55 mM $p = 0.004$) and number (Control baseline vs. Control KCL 55 mM $p = 0.0225$). In contrast, NL neurons show at baseline reduced Syt1 immunoreactivity (Syt1 intensity: Control baseline vs. NL baseline $p = 0.0001$. Syt1 number: Control baseline vs. NL baseline $p = 0.0464$), and forced depolarization does not increase vesicle release in NL. Experiments were performed in $N = 3$ independent replicates. Data are displayed as Mean $\pm$ SD. (*$p < 0.05$, **$p < 0.01$, ***$p < 0.001$). Scale bar represents 10 μm.

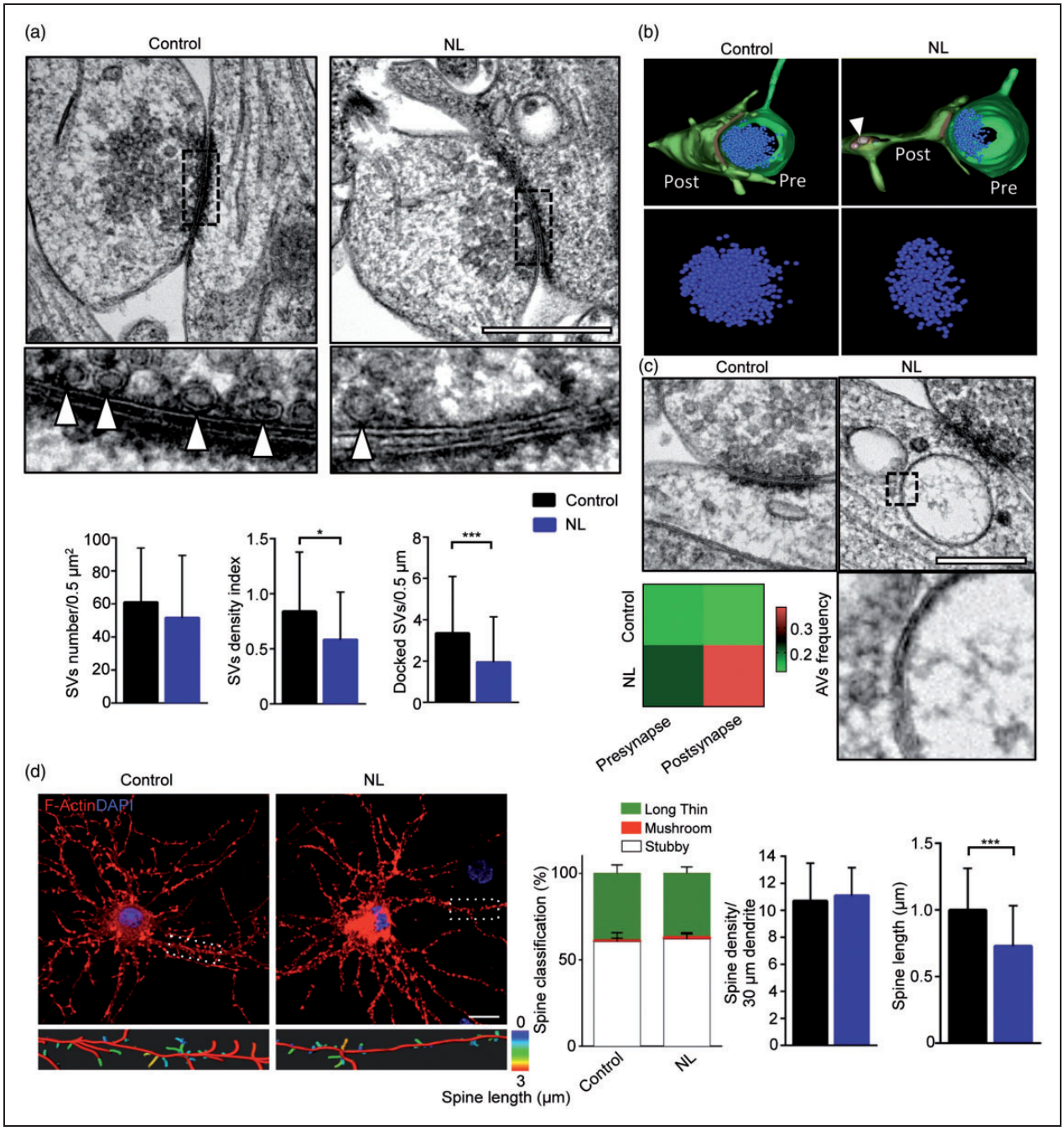

Figure 4. Reduced vesicle density and postsynaptic morphological alterations in NL neurons. (a) Example of electron micrographs of synaptic contacts from Control and NL neurons. NL neurons show reduced clustering of SV at presynaptic boutons (Control vs. NL $p = 0.0465$), as well as a significant reduction of docked SV (Control vs. NL $p < 0.0001$). Higher magnification shows docking vesicles (white arrowheads) at the active zone. (b) Representative 3D reconstruction of transmission electron tomography showing reduced SV clustering in NL synapses (Pre – presynaptic terminal; Post – postsynaptic terminal; arrowhead indicates an AV). (c) Example of electron micrographs of synaptic contacts from Control and NL neurons. NL increases the frequency of AVs at the postsynaptic site (Control vs. NL $p = 0.0148$). The higher magnification shows the typical double membrane characterizing AVs. (d) Representative confocal images of Control and NL neurons overexpressing LifeAct construct to visualize F-Actin (RFP-tagged). Control and NL neurons have comparable number of dendritic spines, but NL reduces the spine length (Control vs. NL $p = 0.0007$). Experiments were performed in $N = 3$ independent replicates. From each independent specimen, 45–50 synapses for condition were evaluated in ultrastractural analysis. Data are displayed as Mean ± SD (*$p < 0.05$, ***$p < 0.001$). Scale bars represent 500 nm in (a) and (c), 15 µm in (d).

We set out to investigate if the induction of autophagy in the postsynaptic side could affect the overall morphology of dendritic spines despite the unmodified PSD. Since reconstruction of spine morphology in sufficient numbers is not feasible in TEM, we investigated hippocampal neurons transfected with the LifeAct-RFP F-actin sensor[42] and imaged with confocal microscopy to quantify spine features.[22] Although spine density (for stubby, mushroom and thin spines, identified according to Risher et al.[52] Figure 4(d)) was comparable in NL and Control neurons both on proximal and distal dendrites, spines exposed to NL appeared to be significantly shorter (Spine length: $0.999 \pm 0.312\,\mu m$ in Control vs. $0.728 \pm 0.303\,\mu m$ in NL, $p = 0.0007$; Figure 4(d)). Taken together, these data show that NL triggers an extensive remodeling of pre and postsynaptic structures.

Rescue of presynaptic Bassoon does not re-establish SV release

Since autophagy has been shown to be a key process induced by NL,[6] we assessed if NL could induce autophagy activation locally in synapses by monitoring the levels of Atg5, which is part of the E3 ligase complex involved in LC3 lipidation.[53] High-resolution confocal images confirmed that Atg5 clusters were localized in close proximity to $MAP2^+$ cytoskeleton, as well as within it, indicating localization also in synapses (Figure 5(a)). In NB^+ condition, in fact, Atg5 clusters could be identified in close proximity of $MAP2^+$ dendrites, but only a minority of synapses (identified by Bassoon staining) were positive for Atg5 ($5.9 \pm 3.88\%$). The density of Atg5 clusters along dendrites increased upon NL (NL: 2.182 ± 0.476 fold of Control, $p < 0.0001$) and a significantly larger fraction of $Bassoon^+$ synapses were associated with Atg5 puncta (19.16 ± 6.329 % in NL; Control vs. NL $p = 0.0475$; Figure 5(a)).

Since Bassoon is a major organizer of the presynaptic active matrix,[51] we wondered if Bassoon degradation could be directly linked to the disorganization of the SV pool and the related functional effects. First, we explored if retrograde signaling[54] from the post-synapse could enhance the stability of the presynaptic architecture and Bassoon levels in NL. To this aim, we overexpressed Shank2-GFP (or GFP alone) in a sparse population of cultured neurons and investigated the loss of Bassoon clusters apposed to Shank2-overexpressing neurons upon NL. Upon NL, Shank2-overexpressing cells displayed only a trend toward reduced loss of Bassoon clusters (NL+GFP vs. NL Shank2 $p = 0.09$; Supplementary Figure S2), implying that cell-autonomous processes regulate loss of Bassoon clusters.

We explored if Bassoon levels could be rescued by blocking either the proteasomal or the autophagic pathway for protein degradation. Hippocampal neurons subject to NL or in Control conditions were co-treated for 5 h either with the autophagy inhibitor 3-MA or the 20 S proteasome inhibitor Bortezomib (PS-341) (or vehicle control, DMSO 0.1%). Interestingly, we found that blockade of autophagy prevented the loss of Bassoon clusters in NL neurons (NL+3-MA: 1.709 ± 0.128 fold of NL+vehicle, $p = 0.0196$; Figure 5(b)) but did not exert any effect in Control conditions. In contrast, co-treatment with the proteasome inhibitor not only prevented the loss of Bassoon clusters in NL (NL+PS-341: 2.268 ± 0.186 fold of NL+vehicle, $p < 0.0001$; NL+PS-341: 1.547 ± 0.186 fold of Control+vehicle, $p = 0.0016$; Figure 5(b)), but also increased Bassoon clusters number above baseline in non-deprived neurons as well (Control+PS-341: 1.284 ± 0.020 fold of Control+vehicle, $p = 0.0487$; Figure 5(b)). These findings suggest that Bassoon is mainly degraded by the ubiquitin-proteasome system, but also that a consistent pool of this scaffold protein is specifically subject to macroautophagy-mediated degradation upon NL.

Finally, we verified if preventing Bassoon loss by autophagy or proteasome blockade was sufficient to restore proper SV release in presynaptic terminals. Interestingly, the intensity (NL+vehicle: 0.701 ± 0.139 fold of Control, $p = 0.0093$; NL+3-MA: 0.743 ± 0.042 fold of Control, $p = 0.0183$; NL + PS-341: 0.703 ± 0.149 fold of Control, $p = 0.082$) and the number (NL + vehicle: 0.668 ± 0.101 fold of Control, $p = 0.005$; NL + 3-MA: 0.640 ± 0.1 fold of Control, $p = 0.0036$; NL+ PS-341: 0.692 ± 0.075 fold of Control, $p = 0.0063$) of $Syt1^+$ terminals were still reduced in NL neurons treated with 3-MA or Bortezomib compared to Control neurons (Figure 5(c)).

Thus, NL effects on presynaptic SV release are extensive and although the loss of Bassoon may be involved in this phenotype, elevation of Bassoon is not sufficient to rescue it.

Reduced SV release is reversed by glucose supplementation independently from restoration of Bassoon levels

Finally, we explored the minimal metabolic requirement for the reversal of the vesicles release loss associated with NL. To this aim, after 3 h of complete NL, hippocampal neurons were exposed to NL medium spiked with a single metabolic substrate: glucose, or the alanine-glutamine dipeptide (henceforth Ala-Gln). Moreover, to investigate the contribution of growth and neurotrophic factors to the NL-induced phenotype, in independent experiments, we added BDNF or insulin to HBSS after the initial 3 h of NL. Interestingly, we observed that glucose addition rescued

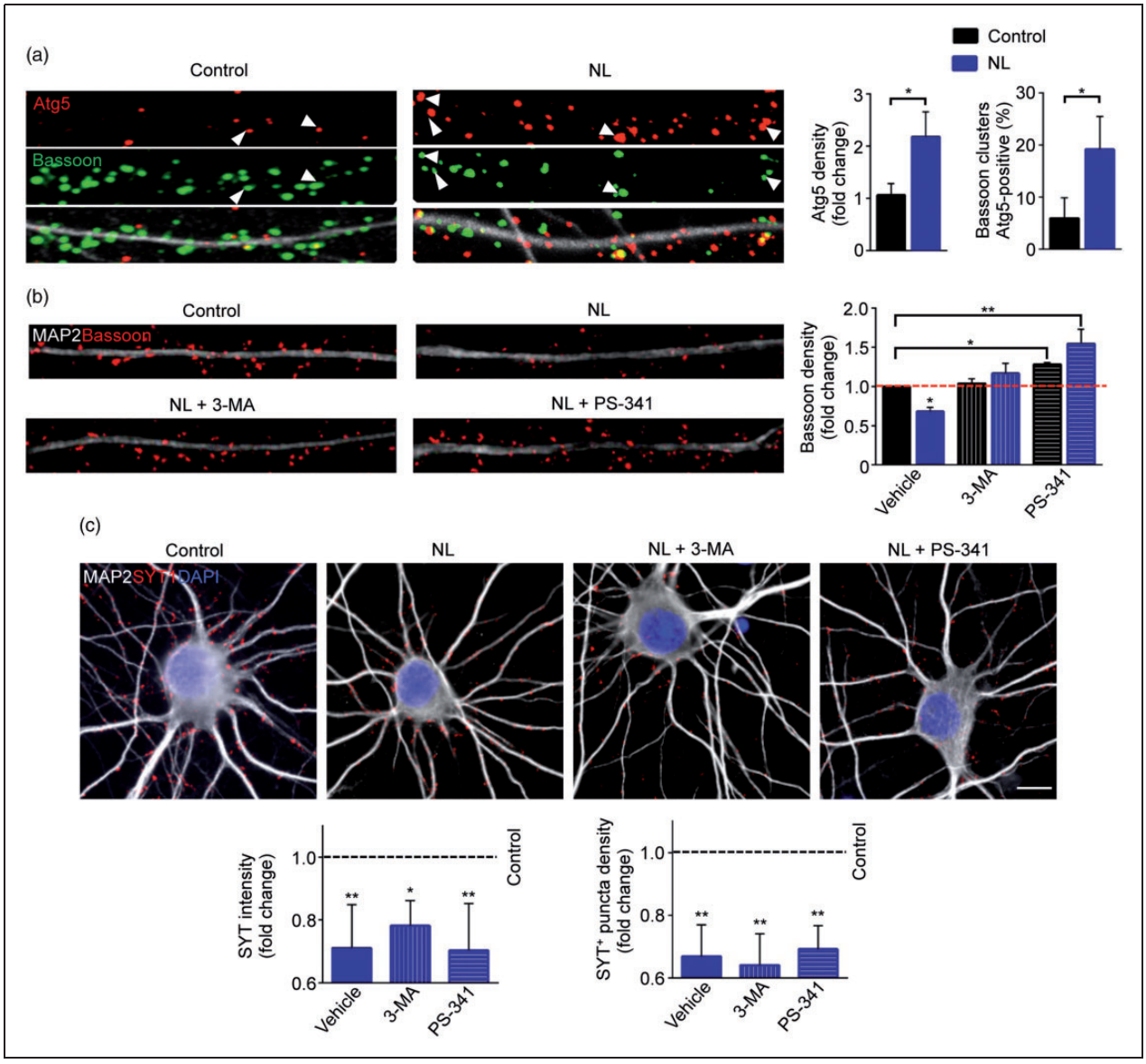

Figure 5. Blocking degradative pathways prevents Bassoon degradation, but not the decrease of SV release. (a) Representative confocal images of dendrites (30 μm) from Control and NL neurons immunostained against MAP2, Atg5 and Bassoon. NL increases Atg5 clusters along the dendrites (Control vs. NL $p = 0.0387$), as well as the number of Bassoon synaptic clusters positive for the autophagic marker (Control vs. NL $p = 0.0475$). (b) Representative images of dendrites (30 μm) from Control and NL neurons. Cells were treated with DMSO (Vehicle), 3-MA or PS-341 and immunostained against MAP2 and Bassoon. Both 3-MA and PS-341 treatments prevent the reduction of bassoon clusters number upon NL (Control + Vehicle vs. NL + Vehicle $p = 0.0196$; Control + Vehicle vs. Control + PS-341 $p = 0.0487$; Control + Vehicle vs. NL + PS-341 $p = 0.0016$; NL + Vehicle vs. NL + 3-MA $p = 0.0034$; NL+Vehicle vs. NL+PS-341 $p < 0.0001$; NL + 3-MA vs. NL + PS-341 $p = 0.0196$). (c) Anti-Synaptotagmin-1 antibody uptake assay was performed in Control and NL neurons treated with DMSO (Vehicle), 3-MA or PS-341. Blocking degradative pathway does not restore SV release (Syt1 intensity: Control+Vehicle vs. NL+Vehicle $p = 0.0093$; Control+Vehicle vs. NL + 3-MA $p = 0.0183$; Control+Vehicle vs. NL+PS-341 $p = 0.0082$. Syt1 numbers: Control+Vehicle vs. NL+Vehicle $p = 0.005$; Control+Vehicle vs. NL+3-MA $p = 0.0036$; Control+Vehicle vs. NL+PS-341 $p = 0.0063$). Experiments were performed in N = 3 independent replicates. Data are displayed as Mean ± SD. (*$p < 0.05$, **$p < 0.01$). Scale bars represent 10 μm in (c).

the intensity (NL+Glucose: 1.537 ± 0.169 fold of NL, $p = 0.0115$) and the numbers (NL+Glucose: 1.258 ± 0.086 fold of NL, $p = 0.008$) of Syt1 puncta when compared to what observed in NL-treated neurons (Figure 6(a)). Moreover, the Ala-Gln dipeptide rescued the release of SV as well, even if less effectively than glucose (NL+Ala-Gln Syt1 intensity: 1.423 ± 0.158 fold of NL, $p = 0.0369$). Of note, supplementation of Gln

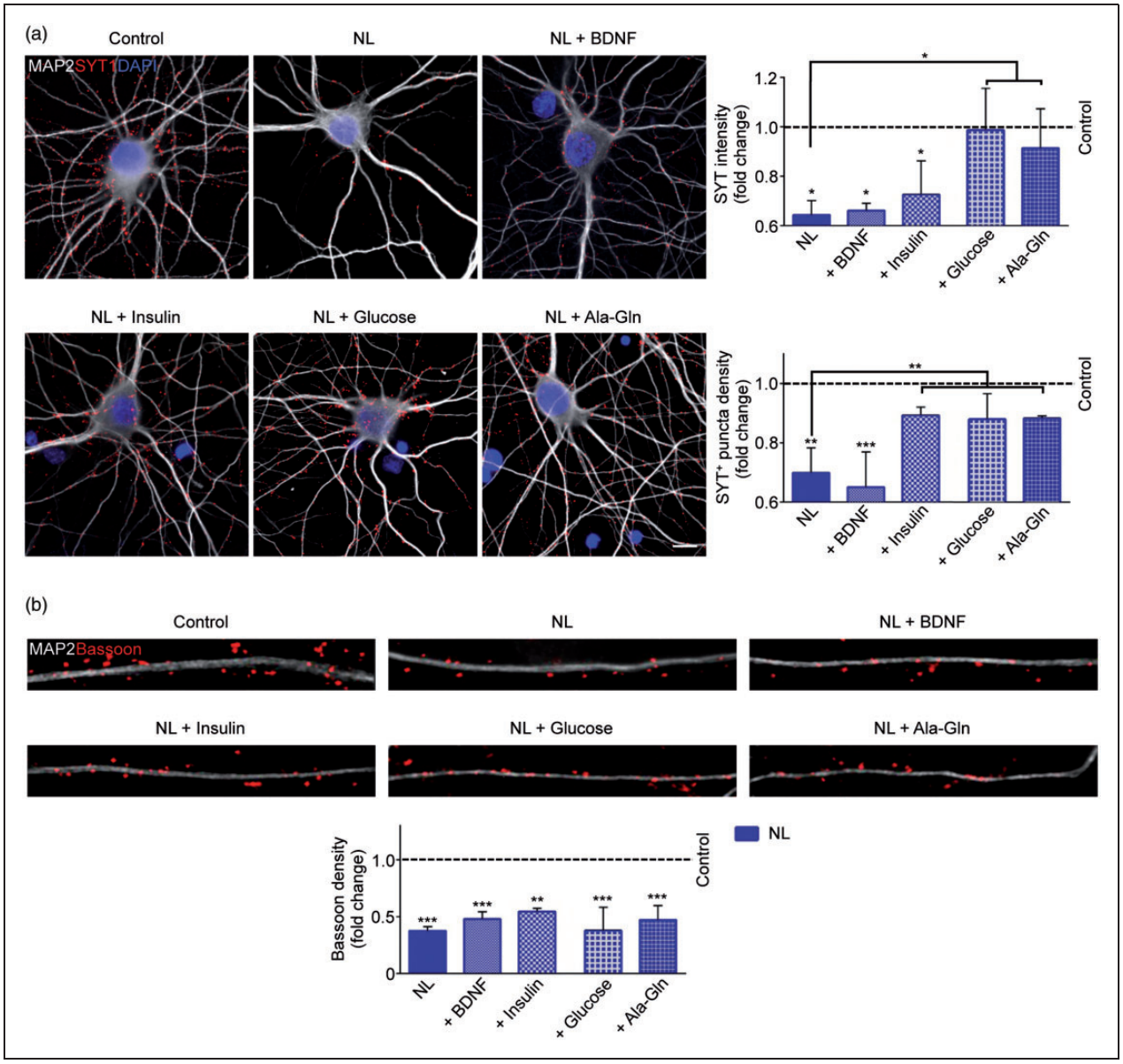

Figure 6. Single metabolite supplementation restores SV release, but not Bassoon levels. (a) Anti-Synaptotagmin-1 antibody uptake assay was performed in Control and NL neurons co-treated for the last 2 h of NL protocol with BDNF, Insulin, Glucose or Ala-Gln. NL neurons fed with glucose and Ala-Gln show rescued SV release, while Insulin exerts a positive effect only on the number of Syt1 clusters (Syt1 Intensity: Control vs. NL $p = 0.0111$; Control vs. BDNF $p = 0.0127$; Control vs. Insulin $p = 0.0346$; NL vs. NL+Glucose $p = 0.0115$; NL vs. NL+Ala-Gln $p = 0.0369$. Syt1 numbers: Control vs. NL $p = 0.0028$; Control vs. NL+BDNF $p = 0.0008$; NL vs. NL+Insulin $p = 0.0053$; NL vs. NL+Glucose $p = 0.008$; NL vs. NL+Ala-Gln $p = 0.0073$). (b) Representative images of dendrites (30 μm) from Control and NL neurons. Cells were co-treated for the last 2 h of NL protocol with Glucose, Ala-Gln, Insulin or BDNF and immunostained against MAP2 and Bassoon. Glucose re-supplementation does not rescue the levels of synaptic Bassoon (Control vs. NL $p = 0.0001$; Control vs. NL+BDNF $p = 0.0006$, Control vs. NL+Insulin $p = 0.0019$; Control vs. NL+Glucose $p = 0.0001$; Control vs. NL+Ala-Gln $p = 0.0006$). Experiments were performed in N = 3 independent replicates. Data are displayed as Mean ± SD. (*$p < 0.05$, **$p < 0.01$, ***$p < 0.001$). Scale bar represents 10 μm in (a).

alone was comparable to Ala-Gln treatment (NL+Gln Syt1 intensity: 1.002 ± 0.009 fold of NL + Ala-Gln, $p = 0.872$; NL + Gln Syt1 numbers: 0.949 ± 0.044 fold of NL + Ala-Gln, $p = 0.512$; data not shown). In contrast, supplementation of BDNF did not rescue neither the number nor the fluorescence intensity of Syt^+ puncta. Interestingly, insulin addition rescued the number of Syt1 clusters in comparison to NL (NL+Insulin: 1.227 ± 0.027 fold of NL, $p = 0.0053$), but did not increase the intensity of those clusters

(Figure 6(a)). Thus, although insulin activated vesicle cycling in a large fraction of synapses, in absence of metabolic substrates, vesicle release remained strongly reduced.

Interestingly, the nutrient-dependent rescue of SV release appeared to be independent from Bassoon's levels: in fact both the re-administration of glucose, or the Ala-Gln treatment, did not restore the number of Bassoon clusters (Figure 6(b)). Of note, BDNF did not rescue Bassoon levels upon NL as well, and re-supplementation of insulin triggered a minor (but still not significant) increase in Bassoon clusters compared to NL.

Finally, we set out to investigate the contribution of Bassoon's autophagic degradation in the reduced release of SV triggered by NL. To this end, neurons were exposed once again to 3 h of NL before adding 3-MA, Ala-Gln, or the combination of the two. The co-treatment with 3-MA and Ala-Gln rescued only as much as Ala-Gln alone the intensity (NL+Ala-Gln: 1.423 ± 0.158 fold of NL, $p = 0.0299$; NL + 3-MA + Ala-Gln: 1.347 ± 0.031 fold of NL, $p = 0.0481$) and the numbers (NL+Ala-Gln: 1.327 ± 0.008 fold of NL, $p = 0.0021$; NL + 3-MA + Ala-Gln: 1.503 ± 0.019 fold of NL, $p < 0.0001$) of $Syt1^+$ puncta, whereas 3-MA alone was ineffective (Supplementary Figure S3(a)). Notably, the co-treatment rescued also the levels of Bassoon (NL+3-MA + Ala-Gln: 1.632 ± 0.182 fold of NL, $p = 0.0470$), but in this case, the effect was comparable to what exerted by 3-MA alone (NL + 3-MA: 1.832 ± 0.013 fold of NL, $p = 0.0018$; Supplementary Figure S3(b)), whereas Ala-Gln alone was ineffective. Taken together, these results confirm that reduced SV release and reduced levels of Bassoon represent distinct events triggered by NL.

Discussion

In this work, we demonstrate that sudden NL results in acute changes in (mainly) presynaptic structure and function, involving rapid and selective degradation of Bassoon, disorganized SV pool, and reduced SV release. Notably, the effect of NL on Bassoon and on SV release can be mechanistically dissociated: the former (but not the latter) depends on autophagy and the latter (but not the former) depends on the limitation of energy substrates. In fact, the impairment in SV release induced by NL is reversible upon nutrient restoration, implying that it is not a sign of degenerating neurons but rather a functional response likely aimed at limiting energy requirements under metabolic stress.

What is the role of the selective Bassoon degradation in the presynaptic response to NL? The single-KO of Piccolo or Bassoon determines no SV clustering phenotype, indicating their functional redundancy, and even the combined KO of Bassoon and Piccolo, characterized by a significant decrease in SV, displays normal electrophysiological responses.[55] According to this redundancy, loss of Bassoon only, upon NL, should not result in a direct effect on SV clustering. In fact, restoration of Bassoon levels by autophagy or proteasome inhibition is not sufficient to rescue the SV release phenotype, whereas re-establishment of SV release by glucose takes place without restoration of Bassoon levels.

Despite Bassoon and Piccolo redundancy, Bassoon-specific functions in presynaptic biology have been reported[56,57]: in particular, Bassoon has been shown to be a negative regulator of autophagy in synapses.[12] Thus, although unrelated to SV release, the loss of Bassoon upon NL may be the initial step toward a more profound disassembly of the presynaptic terminal by autophagy or by ubiquitin/proteasome pathways.[13] Interestingly, autophagy-mediated degradation of Bassoon appears to be an NL-specific response, since under physiological conditions Bassoon is mainly a substrate of proteasomal degradation[58]; actually, Bassoon has not been reported before to be itself an autophagy substrate.

On the other hand, our data show that SV de-clustering is a functional response to NL and that impairment in SV release is independent of Bassoon levels. In fact, SV recycling requires the largest energy expenditure in neuronal physiology[7] and may especially affected by the metabolic stress under NL. In fact, presynaptic glycolysis is critical to maintain SV release under stress in C. Elegans[59]; likewise, blocking local glycolysis or limiting the synaptic access to glucose (by knock-down of the glucose transporter GLUT4) severely slows down SV fusion and recycling.[7,8] At least in C. Elegans, assembly of synaptic glycolytic enzymes metabolons in response to metabolic stress does not take place on SV themselves but rather on the SYD-2 scaffold protein,[59] a member of the active zone matrix similar to Liprin-α[60] which, in turn, interact with Bassoon through ELKs protein.[61,62] Thus, it is possible that loss of presynaptic scaffold proteins may make presynaptic glycolysis less efficient, in particular under metabolic stress. In this direction, insulin, which was shown to suppress NL-induced autophagy,[6] restored a large fraction of SV-releasing synapses although, in absence of glucose restoration, amount of SV released remained very limited.

The vulnerability of the ultrastructure and function of presynaptic terminals observed in our NL model is coherent with observations in TBI and stroke models. In fact, rapid and selective loss of presynaptic proteins such as synaptophysin[63] but not of SNARE factors[64] has been reported in controlled-cortical injury models and acute dysfunction of presynaptic terminals has

been reported in hippocampus subject to fluid-percussion injury[65]; within the limitation of EM performed on pathology specimens, structural damage to the presynaptic terminal has been detected in cortical biopsies from TBI patients.[66] In addition, dysfunction at synaptic level, and in particular in presynaptic terminals, has been reported in stroke models: brief hypoxia is sufficient to block presynaptic vesicle release without loss of membrane potential.[67,68]

Notably, it has been hypothesized that specific dysfunction of presynaptic terminals, rather than damage to whole neurons, may subsume transient neurological deficits in a subset of stroke patients in which gross MRI abnormalities are not observed.[69] Although in vivo experiments provide the best models for translational applications, the multiplicity of concomitant factors (hypoxia, NL, inflammation) makes difficult to disentangle the relative contribution of each of them on synaptic phenotypes. By using an NL-only approach, we have demonstrated that hypoxia is not a prerequisite of presynaptic dysfunction, which can be evoked by the sudden limitation of nutrients alone. Nevertheless, some features of NL appeared to be shared by oxygen/glucose deprivation (OGD) models. In fact, the increase in synaptic levels of the NR1 subunit we have observed is in agreement with the increased NR1 surface expression observed in hippocampal slices upon OGD[70] and thought to be part of long-term potentiation (LTP) of excitatory synapses induced by brief ischemia.[71] Of note, the enrichment in NR1 subunits appears in our model under considerably less severe metabolic stress (no oxygen deprivation, reduced but available glucose). Since in the NL the neurotransmitter release appears to be reduced, one may speculate that the upregulation of NR1 contributes to a homeostatic response aimed at maintaining stable the synaptic input. It is possible to speculate that, under NL, a sudden decrease in overall vesicle release may result into the reduced excitation of principal neurons. Since loss of synaptic excitation (due to reduced vesicle release) may increase neuronal vulnerability,[72] the increased postsynaptic NMDAR response, together with reduced inhibition (leading to an acute change in excitation/inhibition balance), may have a protective goal; however, when left unchecked, this response might contribute to the hyperexcitability of neurons upon metabolic stress and the ensuing seizures (e.g. in hypoglycemia[73] or in the acute phase of traumatic brain injury).[74]

Despite its simplicity, NL triggers a multiplicity of responses affecting differentially the composition of the presynaptic terminal: the induction of autophagy and the metabolic impairment appear to co-exist in the NL model. At least in TBI model, blockade of autophagy has been considered a viable option to prevent neurological damage (structural and functional)[75] and has been associated with a preservation of synaptic proteins.[76] However, our data show that, although autophagy blockade can prevent the loss of specific presynaptic proteins (such as Bassoon), prompt resupply of metabolic substrates appears to be a more effective strategy to restore synaptic function.

Our exploration of the effect of sudden NL on neuronal physiology was focused on synaptic readouts, and in order to make it experimentally tractable, it has been performed in a culture enriched with neurons (only less than 30% of cells were astrocytes). Since astrocytes and other glial cells have been shown to influence and support neuronal metabolic needs,[1,77] the synaptic readouts we have identified provide now an entry point in evaluating how varying ratios of neurons and astrocytes may affect neuronal sensitivity to acute mismatch between required and available metabolic substrates. Of note, glucose, which is directly metabolized at synaptic level,[7] provides a more complete SV release restoration than Ala-Gln, which may require several metabolic steps involving also astrocytes.[78]

It has been reported that the sensitivity of neurons of nutrient deprivation in terms of autophagy induction and survival, and the related adaptive mechanisms, is different in cells derived from male or female animals,[79] although in conditions of more severe deprivation (no glucose, piruvate, glutamine) than those used in this study. Our experimental design did not include a preselection of the embryos and the cultures contain a mixed population of neurons with either genotype; further exploration of gender-related responses to NLs is therefore warranted.

Thus, our data suggest that although treatment of acute synaptic impairment may be a translationally relevant goal in conditions of NL (such as in stroke and TBI),[69] it may require a multi-target strategy: acute restoration of synaptic function may be best achieved by prompt resupply of energy substrates, whereas autophagy impairment may preserve the protein composition of presynaptic terminals.

Funding

The author(s) disclosed receipt of the following financial support for the research, authorship, and/or publication of this article: This work was supported by Deutsche Forschungsgemeinschaft (DFG 1718/7-1) to TMB; by Deutsche Forschungsgemeinschaft as part of the Collaborative Research Center 1149 ''Danger Response, Disturbance Factors and Regenerative Potential after Acute Trauma'' (SFB1149-A02 and SFB1149-B05) to TMB and FR; by the ERANET-NEURON initiative ''External Insults to the Nervous System'' and BMBF as part of the MICRONET consortium (FKZ 01EW1705A) and by the Baustein program of the Medical Faculty of Ulm University to FR.

Acknowledgements

The authors are thankful to Ursula Pika-Hartlaub, Bianca Mekle, Maria Manz and Renate Kunz for the technical support.

Declaration of conflicting interests

The author(s) declared no potential conflicts of interest with respect to the research, authorship, and/or publication of this article.

Authors' contributions

AC and TMB conceived the project. AC, FR and TMB planned the experiments. AC and DG performed experiments and analyzed data. PW provide support and expertise for TEM analysis, and performed 3D reconstruction of synapses. AC and FR wrote the manuscript with help from DG. TMB supervised the work, corrected the manuscript and provided funding and materials

Supplementary material

Supplementary material for this paper can be found at the journal website: http://journals.sagepub.com/home/jcb

ORCID iD

Francesco Roselli http://orcid.org/0000-0001-9935-6899.

References

1. Magistretti PJ and Allaman I. A cellular perspective on brain energy metabolism and functional imaging. *Neuron* 2015; 86: 883–901.
2. Giza CC and Hovda DA. The new neurometabolic cascade of concussion. *Neurosurgery* 2014; 75: S24–S33.
3. Quaegebeur A, Segura I, Schmieder R, et al. Deletion or inhibition of the oxygen sensor PHD1 protects against ischemic stroke via reprogramming of neuronal metabolism. *Cell Metab* 2016; 23: 280–291.
4. Davis EA and Jones TW. Hypoglycemia in children with diabetes: incidence, counterregulation and cognitive dysfunction. *J Pediatr Endocrinol Metab* 1998; 11: 177–182.
5. Won SJ, Jang BG, Yoo BH, et al. Prevention of acute/severe hypoglycemia-induced neuron death by lactate administration. *J Cereb Blood Flow Metab* 2012; 32: 1086–1096.
6. Young JE, Martinez RA and La Spada AR. Nutrient deprivation induces neuronal autophagy and implicates reduced insulin signaling in neuroprotective autophagy activation. *J Biol Chem* 2009; 284: 2363–2373.
7. Rangaraju V, Calloway N and Ryan TA. Activity-driven local ATP synthesis is required for synaptic function. *Cell* 2014; 156: 825–835.
8. Ashrafi G, Wu Z, Farrell RJ, et al. GLUT4 Mobilization supports energetic demands of active synapses. *Neuron* 2017; 93: 606–615.
9. Gundelfinger ED, Reissner C and Garner CC. Role of Bassoon and Piccolo in assembly and molecular organization of the active zone. *Front Synaptic Neurosci* 2016; 7: 19.
10. Davydova D, Marini C, King C, et al. Bassoon specifically controls presynaptic P/Q-type Ca(2+) channels via RIM-binding protein. *Neuron* 2014; 82: 181–194.
11. Wang X, Hu B, Zieba A, et al. A protein interaction node at the neurotransmitter release site: domains of Aczonin/Piccolo, Bassoon, CAST, and rim converge on the N-terminal domain of Munc13-1. *J Neurosci* 2009; 29: 12584–12596.
12. Okerlund NL, Schneider K, Leal-Ortiz S, et al. Bassoon controls presynaptic autophagy through Atg5. *Neuron* 2017; 93: 897–913.
13. Waites CL, Leal-Ortiz SA, Okerlund N, et al. Bassoon and Piccolo maintain synapse integrity by regulating protein ubiquitination and degradation. *EMBO J* 2013; 32: 954–969.
14. Sheng M and Hoogenraad CC. The postsynaptic architecture of excitatory synapses: a more quantitative view. *Annu Rev Biochem* 2007; 76: 823–847.
15. Monteiro P and Feng G. SHANK proteins: roles at the synapse and in autism spectrum disorder. *Nat Rev Neurosci* 2017; 18: 147–157.
16. Bhattacharyya S, Biou V, Xu W, et al. A critical role for PSD-95/AKAP interactions in endocytosis of synaptic AMPA receptors. *Nat Neurosci* 2009; 12: 172–181.
17. MacGillavry HD, Kerr JM, Kassner J, et al. Shank-cortactin interactions control actin dynamics to maintain flexibility of neuronal spines and synapses. *Eur J Neurosci* 2016; 43: 179–193.
18. Sala C, Piëch V, Wilson NR, et al. Regulation of dendritic spine morphology and synaptic function by Shank and Homer. *Neuron* 2001; 31: 115–130.
19. Na CH, Jones DR, Yang Y, et al. Synaptic protein ubiquitination in rat brain revealed by antibody-based ubiquitome analysis. *J Proteome Res* 2012; 11: 4722–4732.
20. Ehlers MD. Activity level controls postsynaptic composition and signaling via the ubiquitin-proteasome system. *Nat Neurosci* 2003; 6: 231–242.
21. Roselli F, Hutzler P, Wegerich Y, et al. Disassembly of shank and homer synaptic clusters is driven by soluble beta-amyloid(1-40) through divergent NMDAR-dependent signalling pathways. *PLoS One* 2009; 4: e6011.
22. Roselli F, Livrea P and Almeida OF. CDK5 is essential for soluble amyloid β-induced degradation of GKAP and remodeling of the synaptic actin cytoskeleton. *PLoS One* 2011; 6: e23097.
23. Schmeisser MJ, Kuhl SJ, Schoen M, et al. The Nedd4-binding protein 3 (N4BP3) is crucial for axonal and dendritic branching in developing neurons. *Neural Dev* 2013; 8: 18.
24. Reim D, Weis TM, Halbedl S, et al. The Shank3 interaction partner ProSAPiP1 regulates postsynaptic SPAR levels and the maturation of dendritic spines in hippocampal neurons. *Front Synaptic Neurosci* 2016; 8: 13.
25. Aguirre-Rueda D, Guerra-Ojeda S, Aldasoro M, et al. Astrocytes protect neurons from $A\beta_{1-42}$ peptide-induced neurotoxicity increasing TFAM and PGC-1 and decreasing PPAR-γ and SIRT-1. *Int J Med Sci* 2015; 12: 48–56.
26. Banker GA and Cowan WM. Rat hippocampal neurons in dispersed cell culture. *Brain Res* 1977; 126: 397–442.
27. Barth A, Nguyen LB, Barth L, et al. Glycine-induced neurotoxicity in organotypic hippocampal slice cultures. *Exp Brain Res* 2005; 161: 351–357.

28. Klinkenberg M, Gispert S, Dominguez-Bautista JA, et al. Restriction of trophic factors and nutrients induces PARKIN expression. *Neurogenetics* 2012; 13: 9–21.
29. Clarke JP and Mearow K. Autophagy inhibition in endogenous and nutrient-deprived conditions reduces dorsal root ganglia neuron survival and neurite growth in vitro. *J Neurosci Res* 2016; 94: 653–670.
30. Boland B, Kumar A, Lee S, et al. Autophagy induction and autophagosome clearance in neurons: relationship to autophagic pathology in Alzheimer's disease. *J Neurosci* 2008; 28: 6926–6937.
31. Allavena G, Boyd C, Oo KS, et al. Suppressed translation and ULK1 degradation as potential mechanisms of autophagy limitation under prolonged starvation. *Autophagy* 2016; 12: 2085–2097.
32. Wu YT, Tan HL, Shui G, et al. Dual role of 3-methyladenine in modulation of autophagy via different temporal patterns of inhibition on class I and III phosphoinositide 3-kinase. *J Biol Chem* 2010; 285: 10850–10861.
33. Willems E, Cabral-Teixeira J, Schade D, et al. Small molecule-mediated TGFβ type II receptor degradation promotes cardiomyogenesis in embryonic stem cells. *Cell Stem Cell* 2012; 11: 242–252.
34. Ivanova D, Dirks A, Montenegro-Venegas C, et al. Synaptic activity controls localization and function of CtBP1 via binding to Bassoon and Piccolo. *EMBO J* 2015; 34: 1056–1077.
35. Heise C, Gardoni F, Culotta L, et al. Elongation factor-2 phosphorylation in dendrites and the regulation of dendritic mRNA translation in neurons. *Front Cell Neurosci* 2014; 8: 35.
36. Wendholt D, Spilker C, Schmitt A, et al. ProSAP-interacting protein 1 (ProSAPiP1), a novel protein of the postsynaptic density that links the spine-associated Rap-Gap (SPAR) to the scaffolding protein ProSAP2/Shank3. *J Biol Chem* 2006; 281: 13805–13816.
37. Schmeisser MJ, Grabrucker AM, Bockmann J, et al. Synaptic cross-talk between N-methyl-D-aspartate receptors and LAPSER1-β-catenin at excitatory synapses. *J Biol Chem* 2009; 284: 29146–29157.
38. Schmeisser MJ, Baumann B, Johannsen S, et al. IκB kinase/nuclear factor κB-dependent insulin-like growth factor 2 (Igf2) expression regulates synapse formation and spine maturation via Igf2 receptor signaling. *J Neurosci* 2012; 32: 5688–5703.
39. Toné S, Sugimoto K, Tanda K, et al. Three distinct stages of apoptotic nuclear condensation revealed by time-lapse imaging, biochemical and electron microscopy analysis of cell-free apoptosis. *Exp Cell Res* 2009; 313: 3635–3644.
40. Nguyen SM, Lieven CJ and Levin LA. Simultaneous labeling of projecting neurons and apoptotic state. *J Neurosci Methods* 2008; 161: 281–284.
41. Herbert AD, Carr AM and Hoffmann E. FindFoci: a focus detection algorithm with automated parameter training that closely matches human assignments, reduces human inconsistencies and increases speed of analysis. *PLoS One* 2014; 9: e114749.
42. Riedl J, Crevenna AH, Kessenbrock K, et al. Lifeact: a versatile marker to visualize F-actin. *Nat Methods* 2008; 5: 605–607.
43. Villinger C, Schauflinger M, Gregorius H, et al. Three-dimensional imaging of adherent cells using FIB/SEM and STEM. *Methods Mol Biol* 2014; 1117: 617–638.
44. Kremer JR, Mastronarde DN and McIntosh JR. Computer visualization of three-dimensional image data using IMOD. *J Struct Biol* 1996; 116: 71–76.
45. Clarkson C, Antunes FM and Rubio ME. Conductive hearing loss has long-lasting structural and molecular effects on presynaptic and postsynaptic structures of auditory nerve synapses in the cochlear nucleus. *J Neurosci* 2016; 36: 10214–10227.
46. Backues SK, Chen D, Ruan J, et al. Estimating the size and number of autophagic bodies by electron microscopy. *Autophagy* 2014; 10: 155–164.
47. Galluzzi L, Baehrecke EH, Ballabio A, et al. Molecular definitions of autophagy and related processes. *EMBO J* 2017; 36: 1811–1836.
48. Maday S and Holzbaur ELF. Compartment-specific regulation of autophagy in primary neurons. *J Neurosci* 2016; 36: 5933–5945.
49. Tsukada M and Ohsumi Y. Isolation and characterization of autophagy-defective mutants of Saccharomyces cerevisiae. *FEBS Lett* 1993; 333: 169–174.
50. Klionsky DJ, Abdelmohsen K, Abe A, et al. Guidelines for the use and interpretation of assays for monitoring autophagy (3rd edition). *Autophagy* 2016; 12: 1–222.
51. Frank T, Rutherford MA, Strenzke N, et al. Bassoon and the synaptic ribbon organize Ca^{2+} channels and vesicles to add release sites and promote refilling. *Neuron* 2010; 68: 724–738.
52. Risher WC, Ustunkaya T, Alvarado JS, et al. Rapid Golgi analysis method for efficient and unbiased classification of dendritic spines. *PLoS One* 2014; 9: e107591.
53. Mizushima N, Noda T, Yoshimori T, et al. A protein conjugation system essential for autophagy. *Nature* 1998; 395: 395–398.
54. Tao HW and Poo M. Retrograde signaling at central synapses. *Proc Natl Acad Sci U S A* 2001; 98: 11009–11015.
55. Mukherjee K, Yang X, Gerber SH, et al. Piccolo and bassoon maintain synaptic vesicle clustering without directly participating in vesicle exocytosis. *Proc Natl Acad Sci U S A* 2010; 107: 6504–6509.
56. Dick O, Tom Dieck S, Altrock WD, et al. The presynaptic active zone protein bassoon is essential for photoreceptor ribbon synapse formation in the retina. *Neuron* 2003; 37: 775–786.
57. Regus-Leidig H, Fuchs M, Löhner M, et al. In vivo knockdown of Piccolino disrupts presynaptic ribbon morphology in mouse photoreceptor synapses. *Front Cell Neurosci* 2014; 8: 259.
58. Lazarevic V, Schöne C, Heine M, et al. Extensive remodeling of the presynaptic cytomatrix upon homeostatic adaptation to network activity silencing. *J Neurosci* 2011; 31: 10189–10200.
59. Jang S, Nelson JC, Bend EG, et al. Glycolytic enzymes localize to synapses under energy stress to support synaptic function. *Neuron* 2016; 90: 278–291.
60. Südhof TC. The presynaptic active zone. *Neuron* 2012; 75: 11–25.

61. Held RG, Liu C and Kaeser PS. ELKS controls the pool of readily releasable vesicles at excitatory synapses through its N-terminal coiled-coil domains. *Elife* 2016; 5: e14862.
62. Wong MY, Liu C, Wang SSH, et al. Liprin-α3 controls vesicle docking and exocytosis at the active zone of hippocampal synapses. *Proc Natl Acad Sci U S A* 2018; 115: 2234–2239.
63. Ding JY, Kreipke CW, Schafer P, et al. Synapse loss regulated by matrix metalloproteinases in traumatic brain injury is associated with hypoxia-inducible factor-1α expression. *Brain Res* 2009; 1268: 125–134.
64. Carlson SW, Yan H, Ma M, et al. Traumatic brain injury impairs soluble N-ethylmaleimide-sensitive factor attachment protein receptor complex formation and alters synaptic vesicle distribution in the hippocampus. *J Neurotrauma* 2016; 33: 113–121.
65. Reeves TM, Kao C, Phil LL, et al. Presynaptic excitability changes following traumatic brain injury in the rat. *J Neurosci Res* 2000; 60: 370–379.
66. Castejòn OJ, Valero C and Dìaz M. Synaptic degenerative changes in human traumatic brain edema. An electron microscopic study of cerebral cortical biopsies. *J Neurosurg Sci* 1995; 39: 47–65.
67. Sun MK, Xu H and Alkon DL. Pharmacological protection of synaptic function, spatial learning, and memory from transient hypoxia in rats. *J Pharmacol Exp Ther* 2002; 300: 408–416.
68. Hershkowitz N, Katchman AN and Veregge S. Site of synaptic depression during hypoxia: a patch-clamp analysis. *J Neurophysiol* 1993; 69: 432–441.
69. Hofmeijer J and VanPutten MJ. Ischemic cerebral damage: an appraisal of synaptic failure. *Stroke* 2012; 43: 607–615.
70. Wang N, Chen L, Cheng N, et al. Active calcium/calmodulin-dependent protein kinase II (CaMKII) regulates NMDA receptor mediated postischemic long-term potentiation (i-LTP) by promoting the interaction between CaMKII and NMDA receptors in ischemia. *Neural Plast* 2014; 2014: 827161.
71. Dias RB, Rombo DM, Ribeiro JA, et al. Ischemia-induced synaptic plasticity drives sustained expression of calcium-permeable AMPA receptors in the hippocampus. *Neuropharmacology* 2012; 65: 114–122.
72. Bading H. Therapeutic targeting of the pathological triad of extrasynaptic NMDA receptor signaling in neurodegenerations. *J Exp Med* 2017; 214: 569–578.
73. Reno CM, Skinner A, Bayles J, et al. Severe hypoglycemia-induced sudden death is mediated by both cardiac arrhythmias and seizures. *Am J Physiol Endocrinol Metab*. Epub ahead of print 17 April 2018. DOI: 10.1152/ajpendo.00082.2018.
74. Vespa PM, McArthur DL, Xu Y, et al. Nonconvulsive seizures after traumatic brain injury are associated with hippocampal atrophy. *Neurology* 2010; 75: 792–798.
75. Luo CL, Li BX, Li QQ, et al. Autophagy is involved in traumatic brain injury-induced cell death and contributes to functional outcome deficits in mice. *Neuroscience* 2011; 184: 54–63.
76. Feng Y, Cui Y, Gao JL, et al. Neuroprotective effects of resveratrol against traumatic brain injury in rats: involvement of synaptic proteins and neuronal autophagy. *Mol Med Rep* 2016; 13: 5248–5254.
77. Mächler P, Wyss MT, Elsayed M, et al. In vivo evidence for a lactate gradient from astrocytes to neurons. *Cell Metab* 2016; 23: 94–102.
78. Schousboe A, Scafidi S, Bak LK, et al. Glutamate metabolism in the brain focusing on astrocytes. *Adv Neurobiol* 2014; 11: 13–30.
79. Du L, Hickey RW, Bayir H, et al. Starving neurons show sex difference in autophagy. *J Biol Chem* 2009; 284: 2383–2396.